

# Crystallisation of Lithium Zinc Silicates

## Part 2 *Comparison of the Metastable and Stable Phase Relations and the Properties of the Lithium Zinc Orthosilicates*

A. R. WEST, F. P. GLASSER

*Department of Chemistry, University of Aberdeen, Scotland*

Metastable phases and phase assemblages are commonly encountered in the  $\text{Li}_4\text{SiO}_4\text{-Zn}_2\text{SiO}_4$  system. Typically, the metastable states arise from a failure of the system to remain at equilibrium upon cooling from higher temperatures. Physical data, including X-ray powder patterns, are presented to characterise the metastable phases. The crystallo-chemical relationships between the metastable and stable phases are discussed and used to explain why metastable phases may arise. Many of the features of the metastable phase assemblages can be represented on phase non-equilibrium diagrams.

The possibilities of encountering these and structurally related phases in glass-ceramics are discussed.

### 1. Introduction

In many systems relevant to glass-ceramic formation, the relationship between bulk composition and the nature and quantity of the crystalline phases which appear is known, at least in broad outline. However, further study often shows that the equilibrium crystallisation processes may be more complex, or indeed, that entirely different products might be obtained than would be predicted from the incomplete data which attempt to describe the behaviour of the systems at equilibrium.

In examining the crystallisation products of  $\text{Li}_2\text{O-ZnO-SiO}_2$  glasses, orthosilicates might be expected to occur in a wide range of compositions even those relatively rich in silica. This is because a wide range of compositions have an orthosilicate phase plus silica occurring as compatible phases, as is shown by the general distribution of three-phase triangles. Stewart and Buchi [1] found that two binary orthosilicate phases could co-exist with  $\text{SiO}_2$  over a wide range of ternary compositions. It has been shown in Part 1 of this study that their description of the number and formulae of the orthosilicate phases was incorrect, although their general conclusions as to the co-existence of orthosilicates with silica were correct. It was also found in Part 1 of this study that a number of

orthosilicate phases could be synthesised which appeared to be thermodynamically metastable. These metastable phases were, typically, prepared by either rapid cooling from elevated temperatures or by the annealing at lower temperatures of phases which had been initially crystallised at higher temperatures. Many of these metastable phases were very persistent. Because of the importance to glass-ceramics of thermal treatments which involve both devitrification at subsolidus temperatures, and slow cooling over some ranges of temperatures, it was thought desirable to study these metastable phases in some detail and to provide physical data for their identification.

### 2. Experimental Results and Discussions

#### 2.1. Experimental Techniques

It was necessary to use both dynamic and static techniques in order to study phase transformations which proceeded at rates varying from very slow to essentially instantaneous. Main reliance for detection of phase changes was placed on differential thermal analysis (DTA) and high temperature powder X-ray diffraction (HTXR), as well as on examination at ambient temperature of the products of static heating, which had been either quenched or slowly cooled to ambient. The starting materials and

preparation of orthosilicate mixtures was the same as that described in Part 1.

## 2.2. The Metastable Assemblages

Departures from equilibrium may be judged by comparison of the phase or phases actually encountered with those found at equilibrium; the latter information is summarised in fig. 1. At temperatures close to the solidus, the equilibrium relations on the orthosilicate join are comparatively simple: the stable phases are high- $\text{Li}_4\text{SiO}_4$  and its zinc-containing solid solutions, a wide range of  $\gamma_{\text{II}}$  solid solutions whose ideal composition lies at the 1:1 ratio, and essentially lithium-free  $\text{Zn}_2\text{SiO}_4$ . The stable high-temperature phases may be synthesised either by freezing of orthosilicate liquids or by prolonged sintering of crystalline starting materials. The metastable

phases described here could all be produced by the cooling of these stable, high-temperature phases, or by the annealing at low temperatures of samples initially prepared at higher temperatures. One of the most important metastable features to appear is the failure of  $\gamma_{\text{II}}$  solid solutions having appropriate compositions to invert to  $\beta_{\text{II}}$  upon cooling. This situation is shown in fig. 2, which summarises the sequence of transformations encountered upon cooling of the high-temperature assemblages at rates ranging from 2 to 20° C  $\text{min}^{-1}$ . Towards the slower end of these cooling rates – at 2 to 5° C  $\text{min}^{-1}$  – and at the 1:1 composition some  $\beta$ -phase may appear but, in general, the sluggishness of the  $\gamma \rightarrow \beta$  conversion prevents  $\beta$ -phase from appearing. Instead, a wide range of  $\gamma_{\text{II}}$  solid solutions invert, first to  $\gamma_{\text{I}}$  solid solutions, and

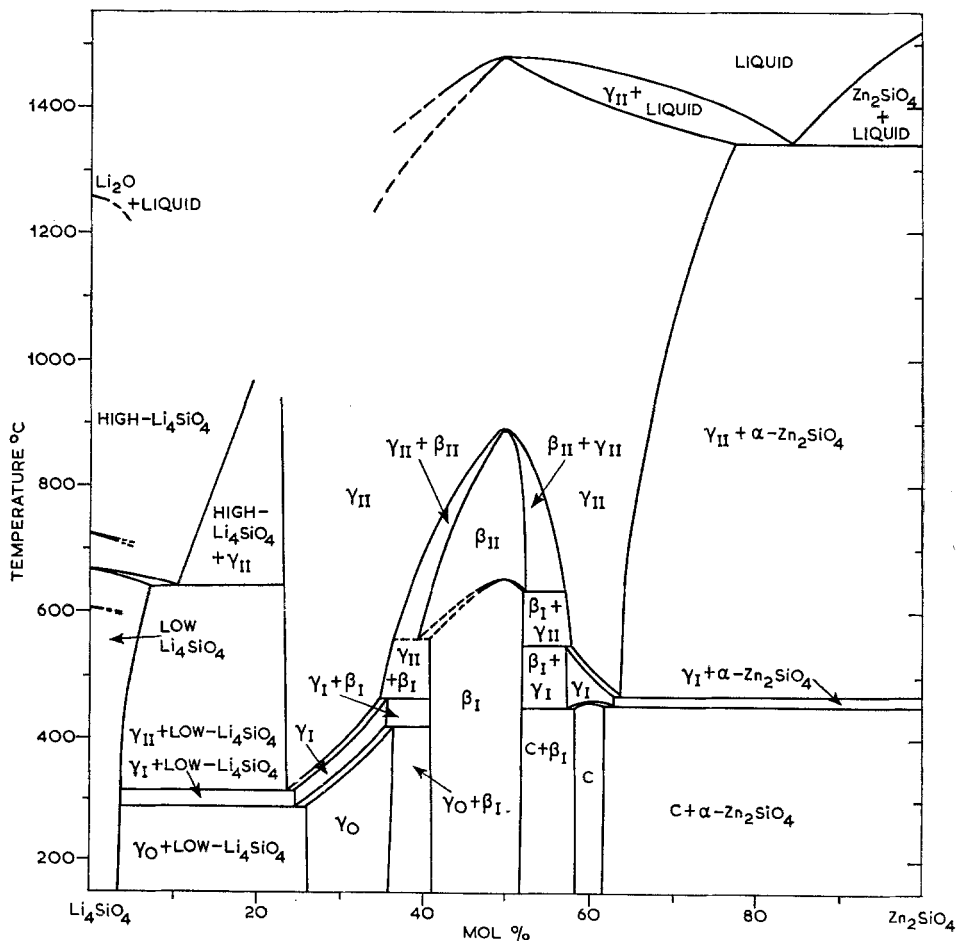


Figure 1 Phase equilibrium diagram for the system  $\text{Li}_4\text{SiO}_4$ - $\text{Zn}_2\text{SiO}_4$ . Incomplete portions of the diagram represent temperature-composition areas which could not be studied, owing to high lithium losses.

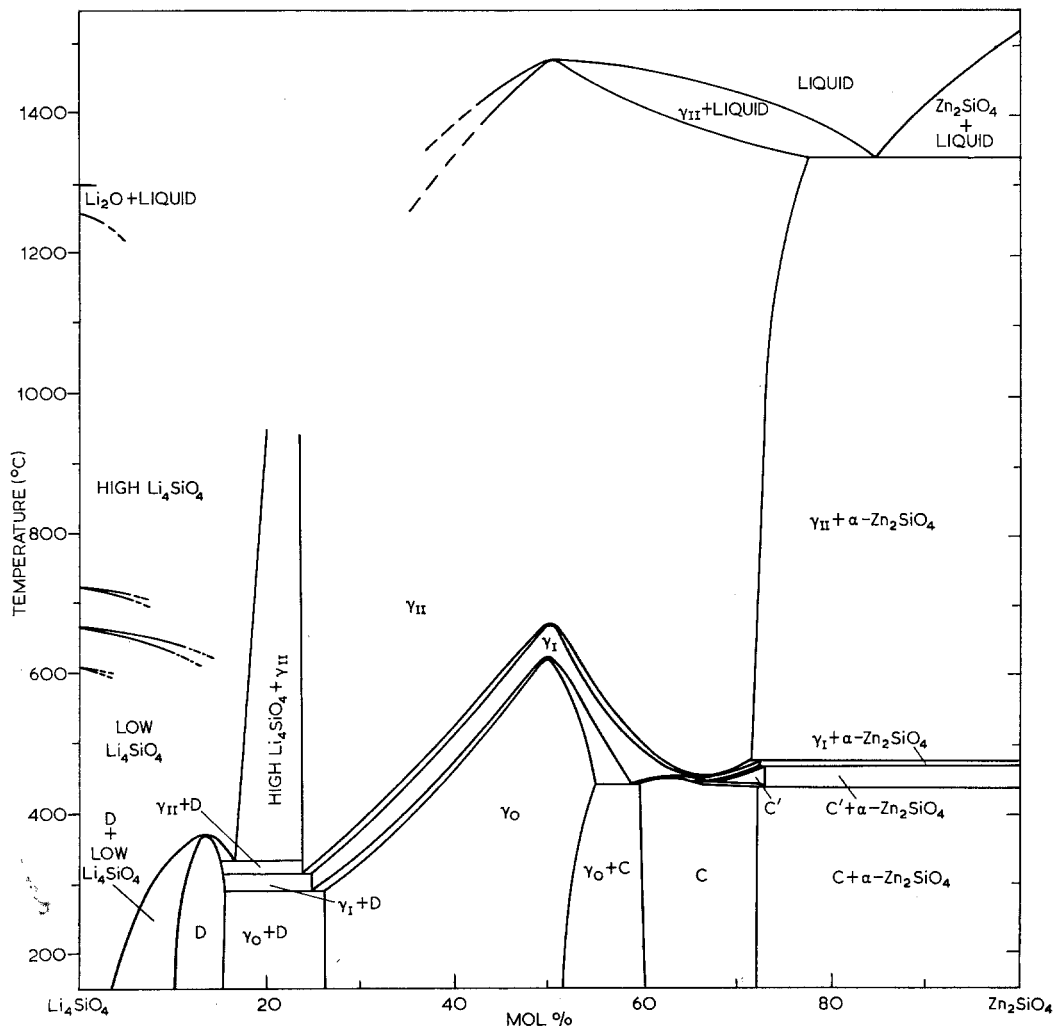


Figure 2 Phase non-equilibrium diagram representing the sequences of transformations encountered in  $\text{Li}_4\text{SiO}_4\text{-Zn}_2\text{SiO}_4$  compositions upon cooling from the liquid, or from solidus temperatures, at moderately slow rates, ranging from approximately 2 to  $20^\circ\text{C min}^{-1}$ .

then to  $\gamma_0$  solid solutions. This sequence of inversions is quite rapid, and the inversions are again encountered reversibly upon reheating. Thus, the  $\gamma$ -family inversions have a quasi-equilibrium character in their extension through the  $\beta$ -phase field. Inversion temperatures for the  $\gamma_{\text{II}} \rightleftharpoons \gamma_{\text{I}}$  and  $\gamma_{\text{I}} \rightleftharpoons \gamma_0$  reactions both pass through thermal maxima, whose positions coincide with the 1:1 composition, at  $670 \pm 5^\circ\text{C}$  and  $630 \pm 10^\circ\text{C}$  respectively. The two-phase regions which must, in a first-order transformation, separate the individual single-phase regions, are very narrow and have not been detected experimentally.

The transformation loops of the  $\gamma$ -phase

inversions, shown in fig. 2, may be regarded as metastable prolongations of those shorter segments which occur on the equilibrium diagram. Not only do these prolongations sweep metastably through the  $\beta$ -field to join smoothly at a thermal maximum, but the  $\gamma_{\text{I}} - \gamma_{\text{II}}$  loop extends towards  $\text{Zn}_2\text{SiO}_4$  to include a wider range of zinc-rich compositions than is possible at equilibrium. This may be explained by the observation that the equilibrium solubility of  $\text{Zn}_2\text{SiO}_4$  in the  $\gamma_{\text{II}}$ -phase decreases markedly with falling temperatures, especially in the temperature interval between the solidus and *ca.*  $1000^\circ\text{C}$ . While the  $\gamma_{\text{II}}$  solid solutions prepared at higher temperatures readily exsolve another phase - in

this instance,  $\text{Zn}_2\text{SiO}_4$  – on slow cooling, rapid cooling or quenching leads to the preservation of metastable solid solutions. These may persist for considerable periods of time at lower temperatures: thus, a solid solution containing 71.5%  $\text{Zn}_2\text{SiO}_4$ \* was held at 430° C for 12 days without any exsolution occurring. The metastable solid solution compositions are, however, free to undergo minor displacive transformations: thus the  $\gamma_{\text{II}} \rightleftharpoons \gamma_{\text{I}}$  phase transformation can be followed reversibly into the metastable region. It is noteworthy that in this region, the inversion temperature passes through a thermal minimum located at  $\sim 67\%$   $\text{Zn}_2\text{SiO}_4$ .

Thus, the  $\gamma$ -family transformation loops in fig. 2 include segments along which the transformations are the thermodynamically stable events, as well as segments which constitute metastable prolongations. The metastable prolongations may, in turn, be divided into two classes. Firstly, a portion occurs in which the  $\gamma$  solid solutions are entirely metastable with respect to another phase. An example of this would be the  $\gamma$  solid solutions close to the 1:1 composition, which are entirely metastable with respect to another phase – in this case,  $\beta$  – having the same composition. Secondly, a metastable portion exists in which the particular composition of the  $\gamma$  solid solution is metastable. The distinction between the two types of metastability is not important with respect to the thermodynamic properties of the system, but it is of importance in considering the kinetics of

transformation to yield the stable phases. In the first case, the solid solutions can convert to the stable phase by homogeneous nucleation of the stable phase, because both phases have the same composition. However, in the second case it is necessary to form heterogeneous nuclei of both the second phases, because each differs in composition from that of the parent solid solution.

The inversion pattern of the metastable zinc-rich  $\gamma_{\text{II}}$  solid solutions is very sensitive to changes in the bulk composition. Over a range of approximately 10%  $\text{Zn}_2\text{SiO}_4$  the inversion pattern changes markedly so that upon cooling, a  $\gamma_{\text{II}}$  solid solution containing *ca.* 62%  $\text{Zn}_2\text{SiO}_4$  first inverts to  $\gamma_{\text{I}}$  and then to a C solid solution, while at the higher zinc contents *ca.* 72%  $\text{Zn}_2\text{SiO}_4$ , a  $\gamma_{\text{II}}$  solid solution inverts to the C-phase via an intermediate phase, which has been designated as the C'-phase because of its similarity to C. As all these events occur within a narrow range of temperatures, DTA is most helpful in interpreting the sequence in which the transformations are encountered for any particular composition, although continuous HTXR patterns are necessary to explain the observed heat effects in structural terms and to identify the phase or phases which are present above and below the inversion temperatures. The appearance of one such HTXR pattern is shown in fig. 3. This pattern was obtained from the composition containing 71.5%  $\text{Zn}_2\text{SiO}_4$ . Prior to the X-ray, the composition was reacted at

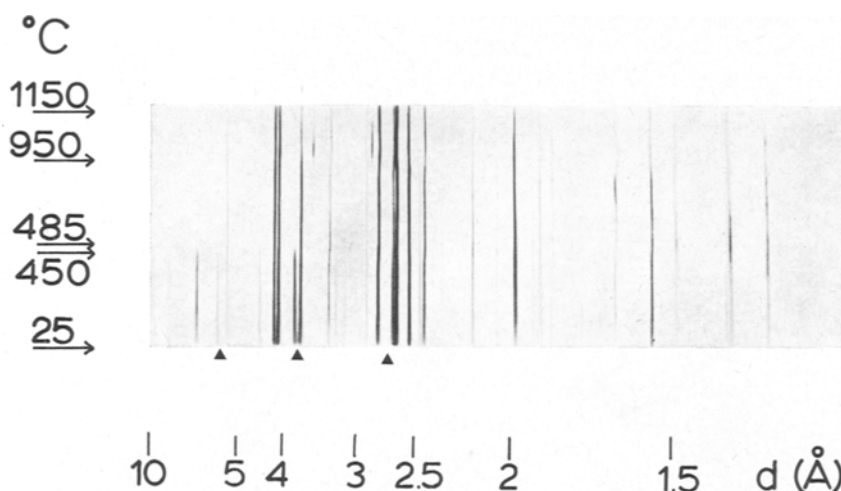


Figure 3 A continuous high-temperature X-ray photograph showing the sequence of phase transformations on reheating a C solid solution containing  $\sim 72\%$   $\text{Zn}_2\text{SiO}_4$  at *ca.*  $1^\circ \text{C min}^{-1}$ .

\*All compositions are given in mole%.

1300° C, cooled rapidly to *ca.* 700° C in order to prevent equilibrium exsolution of  $Zn_2SiO_4$ , and then cooled more slowly to ambient in order to convert the  $\gamma_{II}$  solid solution to the C-phase. The resulting product is thus a homogeneous C solid solution. The distinction between C and C' solid solutions having the same composition involves a search for line splittings, as the C-phase appears to be a distorted, pseudo-orthorhombic modification of the orthorhombic C'-phase. Several of these extra diagnostic reflections which appear in the photograph are indicated by arrows. This sample was heated in the HTXR camera; the rate of temperature rise was not constant, but averaged 1.0° C min<sup>-1</sup>. The first event seen on the photograph is the disappearance of the C-lines at ~ 450° C. Thus, at 450° C, C transforms to a C' solid solution of the same composition. At approximately 485° C, the C' solid solution transforms to a  $\gamma_{II}$  solid solution. In fact, the DTA shows an asymmetric endotherm, indicating that the transformation probably proceeds via  $\gamma_I$  which then converts to  $\gamma_{II}$ , but in this photograph, only  $\gamma_{II}$  is visible. This conversion of C' to  $\gamma_{II}$  produces a major change in the pattern: note, for example, the number of reflections at larger *d*-spacings which either disappear or which change markedly in intensity, and those at smaller *d*-spacings which undergo an acceleration in the rate of change of *d*-spacing with temperature.

At ~ 950° C, the  $\gamma_{II}$  solid solution begins to exsolve willemite. Not only do willemite lines appear, but the  $\gamma_{II}$  lines shift rapidly in *d*-spacing as the exsolution proceeds. With a continued rise in temperature, the quantity of willemite exsolved passes through a maximum. This is because, with rising temperatures, equilibrium is attained more rapidly; this leads to progressively more rapid exsolution. However, with increasing temperatures, the equilibrium of the reaction is shifting towards an increase in the equilibrium solubility of  $Zn_2SiO_4$  in  $\gamma_{II}$  solid solutions. Eventually, this latter factor dominates the reaction and at the highest temperature shown, *ca.* 1150° C, the  $Zn_2SiO_4$  is being rapidly resorbed.

The C'-phase is entirely metastable, and has no place on the equilibrium diagram. It tended to appear only over a limited range of composition, and always near the upper temperature limit of persistence of the C-family phases: thus, it occurs as an intermediate phase in the conversion of  $\gamma_{II}$  solid solutions to C, or vice versa. The range of its

occurrence, as shown in fig. 2, can be followed on the basis of data obtained from both the heating and cooling cycle of HTXR runs. The heat effects associated with both the reactions:  $\gamma_{II} \rightleftharpoons \gamma_I$  solid solutions and  $C \rightleftharpoons C'$  solid solutions, are relatively small; on the other hand, the reactions:  $\gamma_I \rightleftharpoons C$  and  $\gamma_I \rightleftharpoons C'$ , give rise to relatively large heat effects. Most of the reactions which delineate the fields of occurrence of the C- and C'-phases are reversible at the rather slower heating and cooling rates used in HTXR (2 to 5° C min<sup>-1</sup>). However, at the rather faster rates used in DTA there is some hysteresis in the reaction sequences, particularly towards the zinc-rich limits of solid solution, where it becomes possible to retain C' solid solutions to ambient. Thus, of the transformations limiting the fields of C and C', only the  $C \rightleftharpoons C'$  transformation was sometimes too sluggish to be followed on the cooling cycle of DTA runs. Some of these phase transformations, and the heat effects associated with them, are shown in fig. 4: part a compares two DTA traces obtained on the heating cycle.

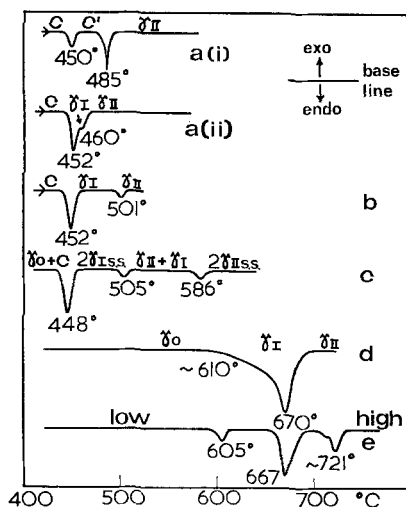


Figure 4 Differential thermal analysis results obtained from some lithium zinc silicates. The heating rate was 15° C min<sup>-1</sup>. See text for the preparation and compositions of samples used. The phases obtained above and below inversions are indicated. In curve (c), the same solid solution phase, but having two different compositions, was found to co-exist, over some ranges of temperatures. This is indicated by "2 $\gamma_{I,SS}$ " etc.

The first trace was obtained from a homogeneous 71.5%  $Zn_2SiO_4$  solid solution, starting as phase C. At 450° C, this inverts to C', giving rise to a

relatively weak endotherm; this C' subsequently inverts to  $\gamma_{II}$  at 485° C, giving a relatively large endotherm. These results corroborate the transformation sequence obtained by HTXR (fig. 3). At ~ 970° C, a broad exotherm appears, due to exsolution of willemite, and the willemite is then progressively resorbed between *ca.* 1020 and 1130° C as indicated by an endothermic drift. These last two events lie outside the range of temperatures shown in fig. 4. If this same, initially homogeneous, solid solution is first annealed at temperatures sufficient to cause exsolution of some  $Zn_2SiO_4$  ( $Zn_2SiO_4$  itself is thermally inactive, but may be detected by powder X-ray methods), a very different DTA trace is obtained. After annealing at 1100° C for 12 to 24 h, this composition was allowed to cool slowly giving, at ambient temperature,  $Zn_2SiO_4$  and a C solid solution whose composition was estimated to be 68%  $Zn_2SiO_4$ . Its pattern of thermal activity is shown in trace a(ii). Upon heating, the C-phase inverts directly to a  $\gamma_I$  solid solution at 452° C and at 460° C the  $\gamma_I$ -phase converts to  $\gamma_{II}$ . The relative size of the heat effects is reversed from that shown in the previous example. Again it should be noted that the actual order of occurrence of the transformations, and hence the interpretation of the DTA, is corroborated by HTXR photographs. These patterns of thermal activity may be contrasted with those obtained from progressively more lithium-rich C solutions. Trace b was obtained on the heating of a C solid solution containing 60%  $Zn_2SiO_4$ . This shows that the endotherm marking the  $\gamma_I$  to  $\gamma_{II}$  inversion has now risen to markedly higher temperatures. A sample at 55%  $Zn_2SiO_4$  was prepared by reaction at 1200° C, followed by slow cooling over 4 h. At ambient temperature, it was found to contain two phases; one, a C solid solution which, from its X-ray *d*-spacings was estimated to have the composition  $59 \pm 2\%$   $Zn_2SiO_4$ , the other, a  $\gamma_0$  solid solution similarly estimated to contain  $54 \pm 2\%$   $Zn_2SiO_4$ . The DTA curve c was obtained on the heating cycle. The two phases invert independently and show no signs of reacting with each other. Thus, the C solid solution inverts to  $\gamma_I$  at 448° C. The transformation of the second phase ( $\gamma_0$ ) to a  $\gamma_I$  solid solution could not be detected by DTA, both because of the small enthalpy change known to be associated with this reaction and also because it was masked by the much larger C  $\rightarrow$   $\gamma_I$  endotherm. However, the existence of two  $\gamma_I$  solid solutions of differing composition is

shown clearly by the next set of endotherms at 505 and 586° C. The 505° C effect represents the transformation of the zinc-rich  $\gamma_I$  solid solution to  $\gamma_{II}$ ; the 586° C effect, the transformation of the zinc-poor  $\gamma_I$ -phase to a  $\gamma_{II}$  solid solution.

The thermal behaviour of the  $\gamma$ -phases at the 1:1 composition shown in trace d is also noteworthy. The onset of the  $\gamma_0 \rightleftharpoons \gamma_I$  transformation is anticipated by a definite endothermic drift; this drift continues to higher temperatures, giving a maximum endothermic deflection at 670° C. Examination of the HTXR photograph shows that 670° C corresponds to the  $\gamma_I \rightleftharpoons \gamma_{II}$  transition which, at this composition, is always rapidly reversible. However, the  $\gamma_0 \rightleftharpoons \gamma_I$  transformation is marked on the HTXR by a definite premonitory region on the low-temperature side of the inversion. The  $\gamma_0$ -phase is probably a monoclinic distortion of the  $\gamma_I$ -phase. It is found that, initially, the degree of monoclinicity of the  $\gamma_0$ -phase decreases only slowly with rising temperature, but about 20 to 30° C below the transformation temperature, it begins to decrease rapidly. Pairs or groups of reflections having symmetry-related indices converge rapidly in the short temperature interval just below the inversion to  $\gamma_{II}$ . This type of evidence supports the contention that the inversion is probably of some thermodynamic order higher than first order. The general diffuse endothermic drift in this temperature range is not due to the existence of a broad two-phase region, the existence of which would be disclosed by the HTXR photographs, but rather, to a marked rise in heat capacity over a short range of temperatures preceding the inversion. It is also noteworthy that in more lithium-rich samples containing  $\gamma_0$ , the monoclinicity of samples examined at ambient temperatures is found to be a function of the cooling history. Slow cooling or brief annealing of samples at lower temperatures produces more monoclinic distortion than is obtained by fast quenching of the same composition. The 1:1 composition exhibited the largest monoclinicity and furthermore, at this composition, the monoclinicity appeared to be independent of thermal history. Prolonged annealing of a range of  $\gamma_0$  solid solutions close to the 1:1 composition is not possible because with longer annealing times they tend to convert to  $\beta$  solid solutions. Thus, it has not been possible to establish the maximum possible monoclinicity of the  $\gamma_0$ -phase.

Mixtures of  $\gamma_0$  and  $\beta$  solid solutions which result from partial conversion of  $\gamma$  have been

obtained. For example, slow cooling of the 1:1 composition from 1100° C to ambient in 4 h gives a mixture of  $\gamma_0$ - and  $\beta$ -phases. The product obtained at ambient has an interesting powder pattern which is distinguished by a continuous diffuse band of scattered X-ray intensity which lies in the angular range between the (002) reflections of the  $\beta_I$ - and  $\gamma_0$ -phases. A study of the mechanism of this transformation by single-crystal methods would be interesting because of the suggestion from the powder data that the transformation probably proceeds by progressive nucleation and coherent growth of regions of the  $\beta$ -phase within the host  $\gamma$ -phase crystals.

The details of the  $\beta_I \rightleftharpoons \beta_{II}$  conversion have been discussed briefly in Part 1. At the 1:1 composition, a minor variant of the  $\beta_{II}$  phase, designated  $\beta_{II}'$ , appears to be stable over a short range of temperatures from approximately 650 to 670° C.  $\beta_{II}'$  forms reversibly as an intermediate phase in the  $\beta_I \rightleftharpoons \beta_{II}$  transformation; it can be preserved to ambient by rapid quenching. However, its occurrence has not been noted in  $\beta$ -phase solid solutions other than the 1:1 composition and its temperature-composition range of occurrence is thus probably very restricted. Because of uncertainty about its compositional extent, it has not been shown in fig. 1. Progressively faster cooling of  $\beta_{II}$  solid solution at the 1:1 composition yields  $\beta_I$  (slow cooling),  $\beta_I'$  and  $\beta_{II}'$ . Upon reheating  $\beta_I'$  at slow rates, it transforms back to  $\beta_I$  before reaching the temperature of the stable  $\beta_I \rightleftharpoons \beta_{II}$  inversion.

In compositions close to  $\text{Li}_4\text{SiO}_4$  an extensive range of  $\text{Li}_4\text{SiO}_4$  solid solutions, containing up to ca. 18%  $\text{Zn}_2\text{SiO}_4$ , are readily preserved metastably to ambient temperature by quenching or rapid cooling. Toward the slower rates of cooling – rates which are, however, still sufficiently fast to prevent exsolution occurring – the solid solutions containing ~ 5% or more  $\text{Zn}_2\text{SiO}_4$  undergo a martensitic type of transformation: this gives rise to the phase designated “phase D”. Powder X-ray data are shown for this phase in table I: although its unit cell size and symmetry are unknown, comparison of the powder data with those of low- $\text{Li}_4\text{SiO}_4$  itself show that D is a superstructure based on  $\text{Li}_4\text{SiO}_4$ . Results obtained by cooling high- $\text{Li}_4\text{SiO}_4$  solid solutions at various rates show that the formation of phase D may not always be a simple, one-step process. For example, at 5%  $\text{Zn}_2\text{SiO}_4$  a homogeneous solid solution allowed to cool spontaneously in air from ca. 900° C, consists of a

low- $\text{Li}_4\text{SiO}_4$  solid solution. Under the same conditions, a solid solution containing 18%  $\text{Zn}_2\text{SiO}_4$  gives, at ambient, a phase whose powder pattern has similarities with those of both low  $\text{Li}_4\text{SiO}_4$  and phase D, but which is clearly not a mixture of the two. It has been designated D'. The D' powder pattern is similar to that of a high- $\text{Li}_4\text{SiO}_4$  solid solution, one conspicuous difference being an additional strong line at  $d = 2.69 \text{ \AA}$ . D' arises from solid solutions whose compositions lie in the metastable region, and the probable sequence of reactions leading to its formation are: high-“ $\text{Li}_4\text{SiO}_4$ ”  $\rightarrow$  low-“ $\text{Li}_4\text{SiO}_4$ ”  $\rightarrow$  D'  $\rightarrow$  D (where “ $\text{Li}_4\text{SiO}_4$ ” refers to solid solutions containing more than 5%  $\text{Zn}_2\text{SiO}_4$ ). At higher zinc contents, progressively faster cooling rates are required to preserve D' to ambient; otherwise it may either convert to D, or exsolve with formation of some  $\gamma$  solid solution. The latter path represents a return to the equilibrium state. The solid solution compositions which give rise to the D-family phases are believed to form by substitution of one zinc and one cation vacancy for a pair of lithium ions and it is suggested that ordering of the (Zn + vacancy) gives rise to the superstructure. The boundaries of the field of phase D have been drawn largely from the results of static heating at temperatures in the range 200 to 400° C, followed by either slow cooling or quenching to ambient, as well as directly, by the appearance of D in the HTXR runs. In order to produce D it is, of course, always necessary to have a  $\text{Li}_4\text{SiO}_4$  solid solution as a starting material: the D-phase has not been formed by direct reaction as, for example, by reacting zinc-free  $\text{Li}_4\text{SiO}_4$  and a zinc-rich orthosilicate mixed in the appropriate ratios. Moreover, if a sample containing phase D is reheated to a temperature just sufficient to cause its decomposition to  $\text{Li}_4\text{SiO}_4$  and  $\gamma_0$ -phases, phase D will not again reform upon cooling. All these lines of evidence point firstly, to the thermodynamic instability of phase D and secondly, to the martensitic nature of the transformation of high  $\text{Li}_4\text{SiO}_4$  solid solutions to yield D.

The reactions involving the formation of phase D could not be followed by DTA, presumably because of the sluggishness of the transformations involved. It is also likely that the enthalpy of its formation from  $\text{Li}_4\text{SiO}_4$  solid solutions is low.

$\text{Li}_4\text{SiO}_4$  itself is thermally active. Its DTA pattern, not previously recorded in the literature, is shown in fig. 4, trace e, and was discussed

more fully in Part 1. It was noted that the high  $\rightleftharpoons$  low transformation apparently became more diffuse with increasing zinc content, as evidenced by the broadening of the DTA exotherm. HTXR shows that, in  $\text{Li}_4\text{SiO}_4$  itself, the high  $\rightleftharpoons$  low transformation is marked only by a rapid – but apparently continuous – change in the  $d$ -spacings and relative intensities of most of the powder lines extending over the temperature range *ca.* 600 to 750° C. With increasing zinc content, this transformation range becomes even less marked and it is progressively more difficult to demonstrate, from any one photograph, that a definite high  $\rightleftharpoons$  low transformation occurs. The

DTA and X-ray evidence shows however, that some sort of transformation, perhaps of a higher thermodynamic order, does extend across the entire range of  $\text{Li}_4\text{SiO}_4$  solid solutions.

Results of cooling at still faster rates, of the order of  $> 50^\circ \text{C min}^{-1}$  and up to an estimated  $500^\circ \text{C min}^{-1}$ , are summarised in fig. 5. At these very fast rates it is not possible to follow the sequence of phase changes directly. The transformation sequence must be inferred by combining information on the phases initially present at the higher temperatures, with information on the phases present after quenching, together with a knowledge of the possible inversion pathways

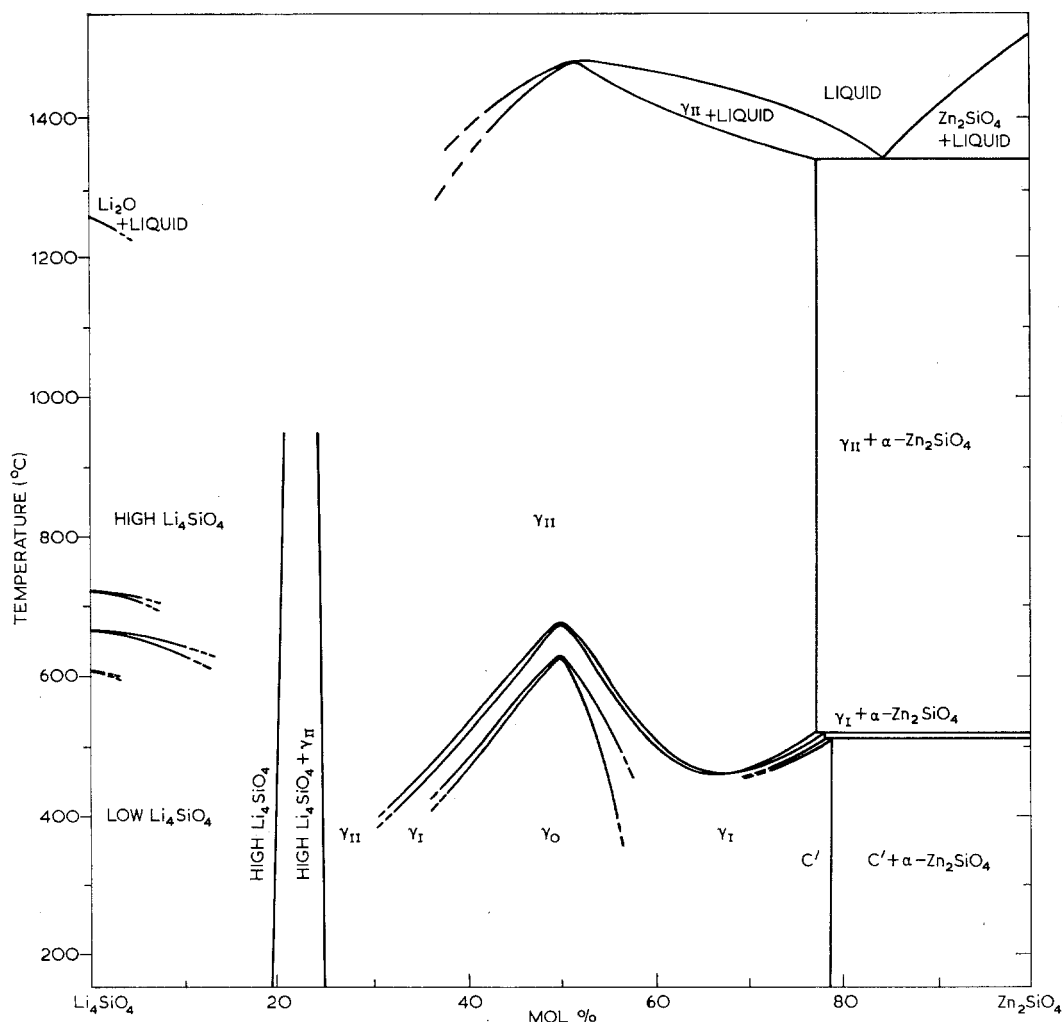


Figure 5 Phase non-equilibrium diagram representing the sequences of transformations encountered in  $\text{Li}_4\text{SiO}_4$ - $\text{Zn}_2\text{SiO}_4$  compositions upon cooling from the liquid or from solidus temperatures at moderately fast rates, ranging from approximately 50 to  $500^\circ \text{C min}^{-1}$ .





the high form with some slight differences attributable to the change in temperature, or if a minor phase change occurred during quenching. In the latter case, the quenched "high" form would have to be considered as a minor structural variant best designated as high'. At these fast quenching rates, phase D does not form.

A range of  $\gamma_{II}$  solid solutions at or close to the lithia-rich limits of solution can be preserved to ambient. The ease of quenching  $\gamma_{II}$  solid solutions may be correlated with the temperature at which the  $\gamma_{II} \rightarrow \gamma_I \rightarrow \gamma_0$  inversions would occur. As these temperatures rise, it becomes progressively more difficult to quench  $\gamma_{II}$ , and  $\gamma_I$  solid solutions are obtained instead. At compositions ranging from ca. 40 to 54%  $Zn_2SiO_4$ , only  $\gamma_0$  is obtained; however, the  $\gamma_{II} \rightarrow \gamma_I$  and  $\gamma_I \rightarrow \gamma_0$  inversion temperatures pass through a thermal maximum at the 1:1 composition and again drop. As they fall,  $\gamma_I$  solid solutions are again obtained. The ease of quenching in  $\gamma_{II}$  or  $\gamma_I$  solid solutions thus correlates well with their apparent lower temperature limit of quasi-equilibrium stability. As this temperature drops, it becomes progressively

easier to preserve the high form by quenching. Finally, at or near the zinc-rich limit of solid solution, C' is obtained as a product of rapid quenching. The two-phase regions separating the fields of C',  $\gamma_0$ ,  $\gamma_I$  and  $\gamma_{II}$ , and especially their terminations against the two-phase regions involving willemite, are not known exactly. Their intersections in fig. 5 are shown schematically.

### 2.3. Thermal Expansion of the Binary Lithium Zinc Silicates

Coefficients of thermal expansion have been calculated to a moderate degree of accuracy from the HTXR photographs. The Guinier-Lenne camera used to record the patterns carries the sample on a metal grid, normally platinum. The reflections from the grid are superimposed on the powder pattern of the sample and after correcting for the known coefficient of thermal expansion of the grid itself, the positions of its X-ray reflections can be used as an internal standard. Temperatures are monitored during the course of the heating or cooling by a platinum/platinum-10% rhodium alloy thermocouple. Provided the powder pattern of the lithium zinc silicate can be

TABLE II Directional coefficients of thermal expansion

(a) $Li_2ZnSiO_4$						
hkl	$\gamma_0^*$			$\gamma_{II}$		
	d(Å) (25° C)	d(Å) (400° C)	d(Å) (620° C)	d(Å) (700° C)	d(Å) (1030° C)	
(200)	3.18	3.19 <sub>5</sub>	3.20 <sub>5</sub>	3.21 <sub>5</sub>	3.23	
(040)	2.67	2.68	2.68 <sub>5</sub>	2.69 <sub>5</sub>	2.70	
(002)	2.53	2.54	2.55	2.56	2.57 <sub>5</sub>	
$\alpha \times 10^{-5} \text{ } ^\circ\text{C}^{-1}$						
a		0.8 ± 0.4	1.1 ± 0.3	1.4 ± 0.2	1.6 ± 0.2	1.8 ± 0.6
b		0.9 ± 0.4	1.0 ± 0.3	1.1 ± 0.2	1.1 ± 0.2	1.2 ± 0.6
c		0.9 ± 0.4	1.3 ± 0.3	1.7 ± 0.2	1.8 ± 0.2	2.0 ± 0.7
$\Delta T$		25-400° C	25-620° C	25-700° C	25-1030° C	700-1030° C
(b) $Li_4SiO_4$						
hkl*	Low		High			
	d(Å) (25° C)	d(Å) (400° C)	d(Å) (800° C)			
(200)	2.58	2.61	2.61 <sub>5</sub>			
(040)	1.528	1.545	1.575			
(002)	2.63	2.67 <sub>5</sub>	2.72 <sub>5</sub>			
$\alpha \times 10^{-5} \text{ } ^\circ\text{C}^{-1}$						
a	2.8 ± 0.9	0.5 ± 0.6	1.6 ± 0.2			
b	2.7 ± 0.3	4.9 ± 1.2	3.8 ± 0.2			
c	4.3 ± 1.4	4.8 ± 1.6	4.5 ± 0.5			
$\Delta T$	25-400° C	400-800° C	25-800° C			

\*The pseudo-orthorhombic cell is used.

indexed, reasonably accurate directional coefficients of thermal expansion can be obtained. A selection of coefficients of thermal expansion measured in this way for the  $\gamma$ -phases is shown in table II a. The  $\gamma_I$ -phase is present only over such a short interval of temperature that its coefficient of thermal expansion could not be measured. On the other hand, the volume change attending the  $\gamma_{II} \rightleftharpoons \gamma_I \rightleftharpoons \gamma_0$  inversions is extremely small, and has been averaged into the coefficients of thermal expansion. In general, the coefficients of thermal expansion increase very markedly with increasing temperature, nearly doubling on average between 700 and 1030° C, as compared with 25 to 400° C. The numerical values are comparable with those of other oxides having moderately high coefficients of thermal expansion. Data for the other lithium zinc orthosilicate phases which are not shown are of a comparable order of magnitude and also have values of  $\alpha$  which increase markedly with increasing temperature. The thermal expansion coefficients of  $\text{Li}_4\text{SiO}_4$  given in table II b reveal the anisotropic nature of its expansion, especially over the temperature interval 600 to 750° C. From HTXR photographs, the coefficient is actually negative in the  $a$ -direction over this temperature range. Soga [2] obtained a mean value of  $2.04 \pm 0.02 \times 10^{-5} \text{ C}^{-1}$  between 25 and 400° C, using dilatometric measurements.

#### 2.4. Electrical Conductivity of the Lithium Zinc Silicates

Small cubes measuring approximately 6 mm on edge were pressed at *ca.* 1500 kg  $\text{cm}^{-2}$  from sintered powders which had been previously reacted to produce the desired phase or phases. Platinum-tape electrodes were attached to opposite cube faces using an electrical-grade platinum paste. The cube, with leads attached, was placed in a muffle furnace and the direct current resistance measured at temperature intervals of 15 to 20° C. Owing to limitations of the furnace used in these measurements, the temperatures recorded are probably only accurate to  $\pm 15^\circ \text{C}$ . Measurements were made on both heating and cooling cycles and, within the limitations of temperature measurement and control, and provided no irreversible phase changes occurred in the sample, were reproducible without significant hysteresis. Typical conductivity-temperature curves are shown in fig. 6. All samples show a marked increase in conductivity with increasing temperature. However, the

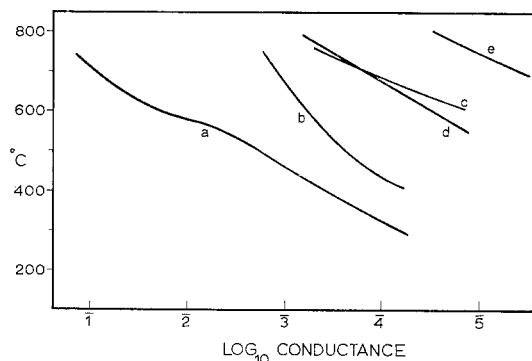


Figure 6 Direct current conductance measurements on some crystalline lithium zinc silicate compacts. Curve (a)  $\text{Li}_4\text{SiO}_4$ ; (b)  $\gamma$  solid solutions, 45%  $\text{Zn}_2\text{SiO}_4$ ; (c)  $\beta$  solid solutions (with some admixed  $\gamma$  solid solutions), 45%  $\text{Zn}_2\text{SiO}_4$ ; (d) C- and  $\gamma$ -phases, 67%  $\text{Zn}_2\text{SiO}_4$ ; (e)  $\text{Zn}_2\text{SiO}_4$ .

relatively low conductivity of  $\text{Zn}_2\text{SiO}_4$  (curve e) is appreciably increased in the phases which contain essential  $\text{Li}^+$ . Thus  $\text{Li}_4\text{SiO}_4$  (curve a) is quite a good conductor at temperatures above *ca.* 600° C. The crystalline structure of the phases also plays a rôle in controlling the conductivity. This effect may be illustrated in two ways. Firstly, conversion of one phase to another phase, where both phases fall in the same family, e.g. the  $\gamma_{II}$ ,  $\gamma_I$  and  $\gamma_0$ -phases, often gives rise to marked inflections in the conductivity-temperature curves. This effect is marked in the change in slope of curve b which was obtained from  $\gamma$ -family solid solutions and which has an inflection at *ca.* 550° C. This inflection occurs in the temperature range of the  $\gamma_{II} \rightleftharpoons \gamma_I \rightleftharpoons \gamma_0$  transformations which would lie between 500 and 600° C for this composition. The change in slope of the  $\text{Li}_4\text{SiO}_4$  curve a seems to lie towards the lower limit of the  $\text{Li}_4\text{SiO}_4$  transition temperatures. The transformation of a phase from one family to another family causes much larger changes in conductivity. Thus, after curve b had been recorded for the  $\gamma$ -family phases, the cube was largely converted to the  $\beta$ -family of phases by holding it at 600° C for 1 week. As shown by curve c this caused a drop in conductivity which, at most temperatures, amounts to nearly two orders of magnitude.

#### 2.5. Discussion

Three types of metastability are found to occur in this system. Firstly, there are homogeneous solid solutions which are found at equilibrium at a certain temperature, but which, upon either

heating or cooling, should enter a two-phase region with a concomitant change in the solid solution composition and production of a second phase. In this case, it is the composition of the solid solution which becomes unstable. In practice, the solution and exsolution reactions are found to be comparatively slow, especially with falling temperatures. An example is the preservation of low- $\text{Li}_4\text{SiO}_4$  solid solutions containing *ca.* 10%  $\text{Zn}_2\text{SiO}_4$  to ambient temperatures. Comparison of figs. 1 and 4 shows that these solid solution composition are unstable at lower temperatures. Secondly, a phase of either fixed or variable composition which is stable at one temperature, may become unstable with respect to another phase or phases upon changing the temperature. In this case it is the phase itself, rather than the particular composition of the phase, which becomes metastable: examples include the preservation, by quenching, to ambient temperatures, of  $\gamma_{\text{II}}$  or  $\gamma_{\text{I}}$  solid solutions, or high- $\text{Li}_4\text{SiO}_4$  solid solutions. Thirdly, phase transformations may occur which result in the formation of a phase which is entirely metastable under all conditions. The formation of phase D is an example: this class of reaction has no expression on the equilibrium diagram, nor can its existence be predicted from the equilibrium diagram. The possibilities of forming metastable phases are increased if departures from equilibrium of the first two types are induced. Many of the metastable pathways are followed reversibly and, because the number of phases present is not more than the maximum permitted by the phase rule, the products obtained constitute a series of quasi-equilibrium states. Phase transformations in the quasi-equilibrium region are thus amenable to the same type of treatment as is accorded to equilibrium transformations. Thus, the data obtained at moderate rates of heating and cooling (fig. 2) do not represent equilibrium, but are nevertheless consistent with a phase diagram which is constructed according to the rules appropriate to an equilibrium phase diagram.

Of all the transformations encountered in this system, only one could not be explained. On heating  $\beta$ -phase of the 1:1 composition an endothermic event was observed on the DTA at  $\sim 960^\circ\text{C}$ , and on cooling, an exotherm at  $\sim 880^\circ\text{C}$ . This same effect was sometimes, but not always, encountered using  $\gamma$ -phases of the 1:1 composition. These effects were not due to  $\gamma \rightleftharpoons \beta$  transformations, as the comparable

HTXR photographs did not show any transformation in this temperature range.

The division of the crystalline phases into families is based partly on the known crystal structures of the end members – low- $\text{Li}_4\text{SiO}_4$  and  $\text{Zn}_2\text{SiO}_4$  – and partly, on the analogy between the various phases having the 1:1 composition and the polymorphs of  $\text{Li}_3\text{PO}_4$ . Comparison of the powder X-ray data would suggest that the crystal structures of all the binary phases thus fall into only three broad structure types or families. One family contains only a single member,  $\text{Zn}_2\text{SiO}_4$ . A second family contains the polymorphs of  $\text{Li}_4\text{SiO}_4$  and phase D. The third family contains the  $\gamma_{\text{II}}$ -,  $\gamma_{\text{I}}$ -,  $\gamma_0$ -,  $\beta_{\text{II}}$ -,  $\beta_{\text{II}}'$ -,  $\beta_{\text{I}}$ -,  $\beta_{\text{I}}'$ -, C- and C'-phases. However, if the range of compositions characteristic of each of the phases is also taken into account, this family can be further sub-divided. Evidence has been presented that the  $\gamma_{\text{II}}$ - and  $\beta_{\text{II}}$ -phases have the 1:1 ratio ( $\text{Li}_2\text{ZnSiO}_4$  composition) as their ideal formulae; the same is probably true of the  $\gamma_{\text{I}}$ -,  $\gamma_0$ -,  $\beta_{\text{II}}'$ -,  $\beta_{\text{I}}$ - and  $\beta_{\text{I}}'$ -phases. However, the C- and C'-phases characteristically occur only at high zinc compositions. The ideal composition – if such exists – for the C-phase lies at  $\sim 62.5\%$   $\text{Zn}_2\text{SiO}_4$  and for the C'-phase, at  $\sim 75\%$   $\text{Zn}_2\text{SiO}_4$ . Neither phase has been prepared at the 1:1 composition and, for this reason, they may be classified into a separate sub-family. This latter distinction also helps to reconcile the results of the present study with those of previous workers whose identification of phases was discussed in the first part of this paper.

## 2.6. Application to Glass-Ceramics

The connection between phase transformations and the volume stability of dense ceramics is well appreciated. Comparison of figs. 1, 2 and 5 shows that, except under conditions of extremely rapid cooling which can only be obtained on a laboratory scale, lithium zinc orthosilicates must undergo one or more phase transformations upon cooling from, say,  $900^\circ\text{C}$ . In the case of first order transformations, e.g.  $\gamma_{\text{II}} \rightleftharpoons \beta_{\text{II}}$ , there will be an appreciable volume discontinuity; in the case of higher-order transformations, e.g.  $\gamma_0 \rightleftharpoons \gamma_{\text{I}}$ , there will be no volume discontinuity, but instead, a range of temperatures over which the coefficients of thermal expansion will undergo a markedly accelerated rate of change. While it may not be possible to suppress inversions completely, it may be possible to control, or systematically choose, the desired phase composi-

tion and hence, the volumetric changes, by controlling the thermal history. Thus it has been shown how, for the 1:1 composition, four different phases all having the same composition can be obtained at ambient temperatures by appropriate choice of cooling conditions. This new knowledge concerning the wide limits of solid solution on the orthosilicate join also calls into question the state of knowledge concerning the  $\text{Li}_2\text{O-ZnO-SiO}_2$  system. Inasmuch as calculations of phase yields are often based on phase diagrams, the information previously available in the literature is probably unreliable for this purpose. Furthermore, the complex polymorphism of the orthosilicates – both equilibrium and non-equilibrium – must have some expression in ternary mixtures containing orthosilicates and other lithia-zinc oxide-silica phases. These relationships are currently being explored.

A knowledge of the crystal chemistry of these orthosilicates may also be useful in predicting the action of nucleating agents. Thus,  $\text{P}_2\text{O}_5$  has been widely used as a nucleating agent in the crystallisation of lithia-silica and lithia-zinc oxide-silica glasses. Its action may well be to form a crystalline phosphate phase which then nucleates an

isostructural silicate. This would suggest that other substances which have related crystal structures, for example, vanadates and arsenates, might have an effect similar to “ $\text{P}_2\text{O}_5$ ” in nucleating an orthosilicate in lithia-containing systems which could yield phases having  $\text{Li}_3\text{PO}_4$ -type structures. The choice of silicate systems which might be expected to contain phases isostructural with one or both forms of  $\text{Li}_3\text{PO}_4$  would include  $\text{Li}_2\text{O-MgO-SiO}_2$  and  $\text{Li}_2\text{O-BeO-SiO}_2$ . A reconnaissance of compound formation and orthosilicate crystal chemistry within these systems is also being undertaken.

### Acknowledgement

The financial support of the Science Research Council is gratefully acknowledged. One of us (A.R.W.) has a University Studentship from the Robbie, Japp and Coutts Funds.

### References

1. I. M. STEWART and G. J. P. BUCHI, *Trans. Brit. Ceram. Soc.* **61** (1962) 615.
2. N. SOGA, *J. Amer. Ceram. Soc.* **47** (1964) 469.

Received 24 March and accepted 14 May 1970